Supplement of Atmos. Chem. Phys. Discuss., 15, 18225–18284, 2015
http://www.atmos-chem-phys-discuss.net/15/18225/2015/
doi:10.5194/acpd-15-18225-2015-supplement

Atmospheric Chemistry and Physics Discussions

Supplement of

Fourteen months of on-line measurements of the non-refractory submicron aerosol at the Jungfraujoch (3580 m a.s.l.) – chemical composition, origins and organic aerosol sources

R. Fröhlich et al.

Correspondence to: A. Prévôt (andre.prevot@psi.ch)

Table S1. Applied a value ranges with reasoning.

season	a range HOA	reason for a range	a range BBOA	reason for a range
summer 2012	0.1–0.7	$a < 0.1$: no good separation OOAs $a > 0.7$: mixing HOA & OOA	–	
autumn 2012	0.0–0.4	$a > 0.4$: mixing HOA & OOA	–	
winter 2012 / 2013	0.0–0.5	$a > 0.5$: mixing HOA & BBOA	0.0–0.1	$a > 0.1$: decrease of m/z 60 & mixing OOA & BBOA
spring 2013	0.3–0.5	$a < 0.3$: large background in $\mathrm{POA_{loc}}$ $a > 0.5$: mixing HOA & OOA	–	
summer 2013	0.0–0.4	$a < 0.3$: worse separation OOAs	0.0–0.4	$a > 0.4$: mixing HOA & BBOA

Table S2. Ratios of HOA to EBC for all seasons.

season	BBOA	HOA	$\mathrm{POA_{loc}}$	OOA (I/II)
summer 2012	–	2.6 %	1.2 %	8.1 % / 8.1 %
autumn 2012	–	6.5 %	2.3 %	0.3 %
winter 2012 / 2013	4.9 %	6.0 %	2.5 %	0.8 %
spring 2013	–	11.1 %	5.9 %	1.1 %
summer 2013	8.9 %	2.4 %	1.1 %	1.5 % / 2.1 %

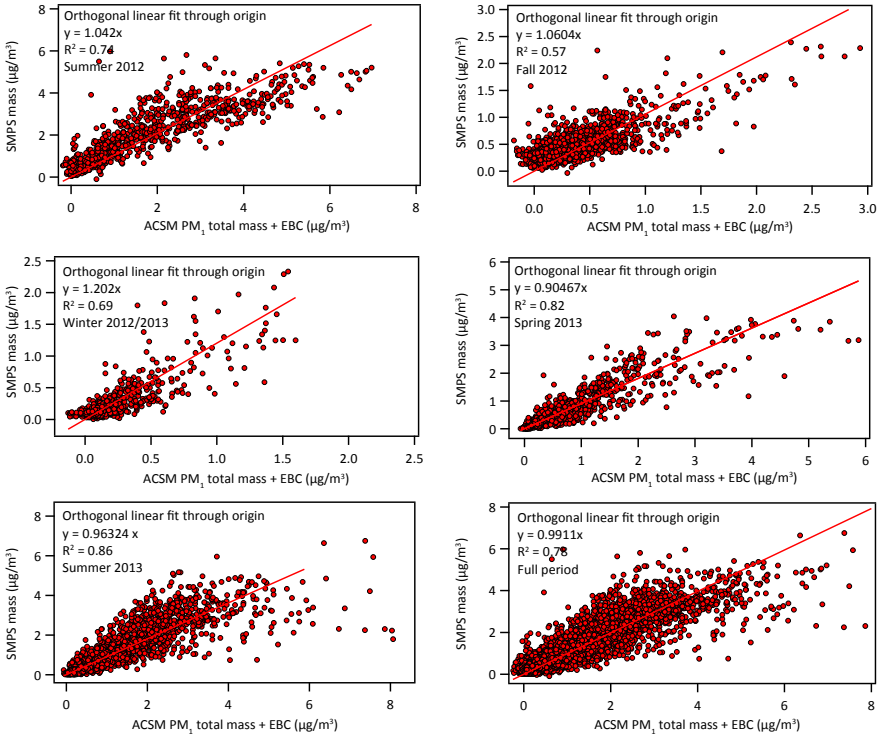

Fig. S1. Correlation plots of mass estimated from the SMPS measurements versus mass measured by the ToF-ACSM plus equivalent black carbon in µg/m^3 for all seasons. The bottom right panel shows the correlation for the full period. Slopes close to 1 all over the year lead to a constant collection efficiency of 1.

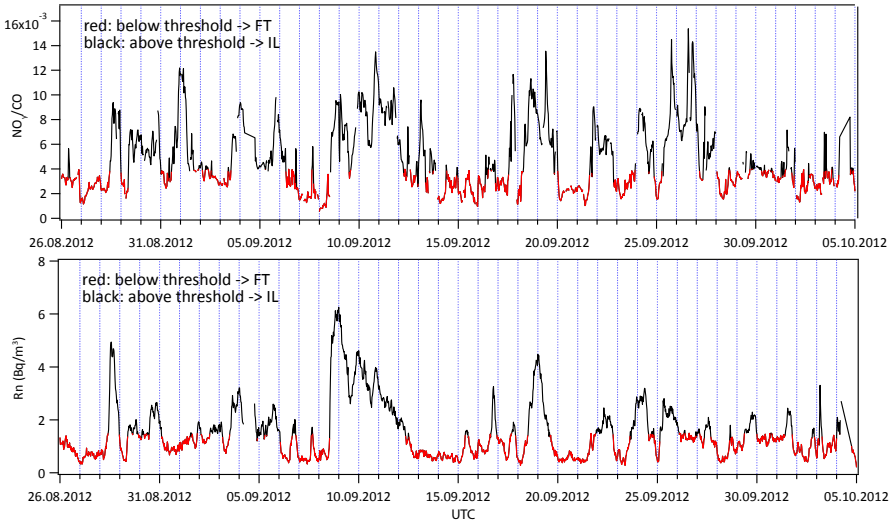

Fig. S2. NO_y/CO (upper panel) and ^{222}Rn concentrations during the same >1-month example period. Applied thresholds are indicated in red. Concentrations above the threshold are considered influenced by PBL air masses. A comparison shows largely the same result for both criteria with ^{222}Rn showing slightly more PBL influence.

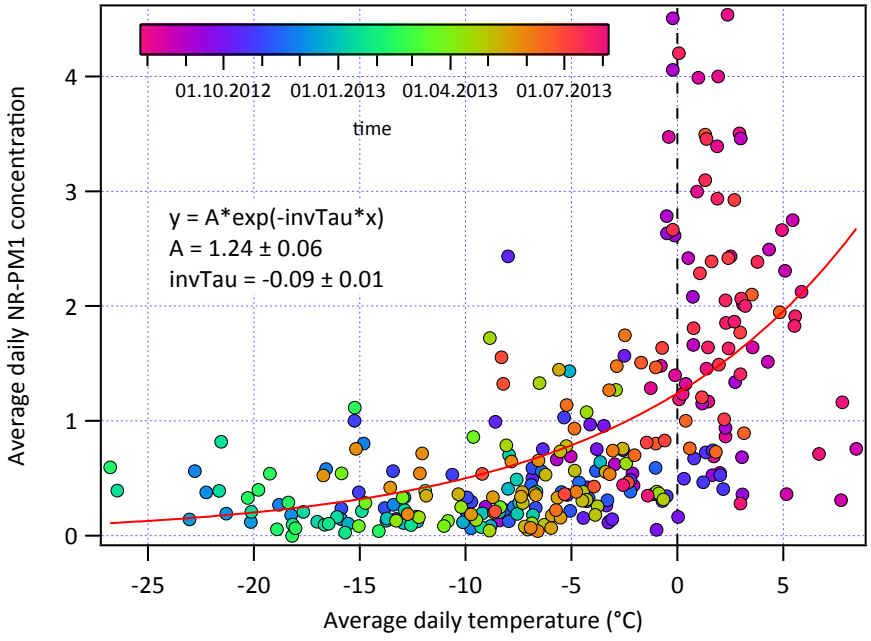

Fig. S3. Daily average PM_1 in $\mu g/m^3$ plotted against daily average temperature T in °C. Data is coloured by date. A strong exponential increase at above zero temperatures is observed. It is noted that obviously the exponential function must level off when full vertical mixing with PBL air is reached.

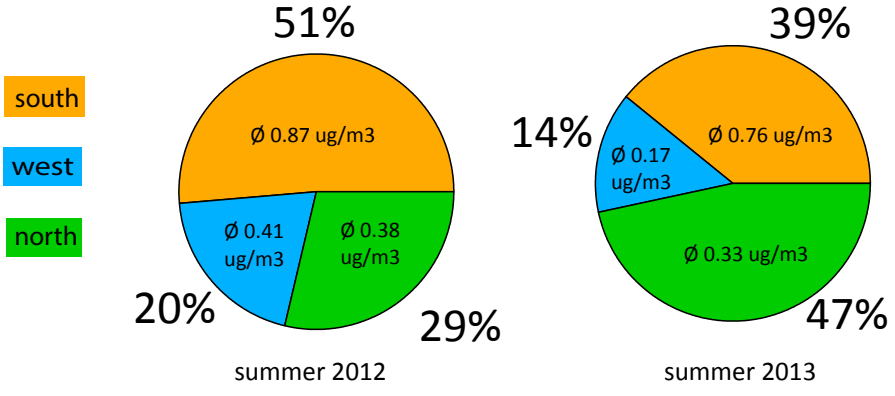

Fig. S4. Frequency of air mass origin during summer 2012 (left) and 2013 (right) including average mass concentrations. Air mass origin was calculated according to the description in Sect. 2.5. North includes clusters #6 & #7, south includes clusters #3, #4 & #5 and west includes cluster #2 as shown in Fig. 5.

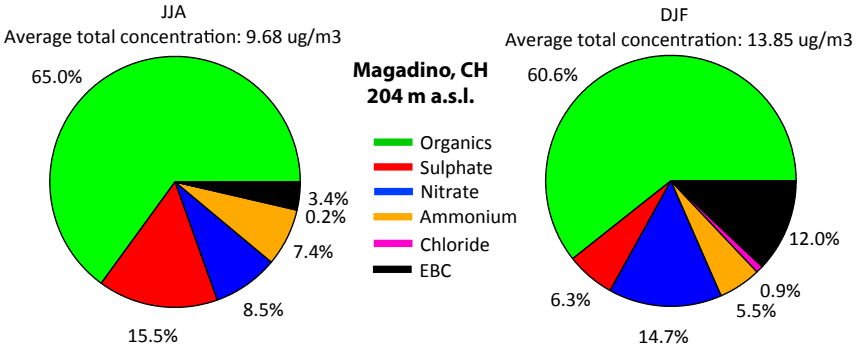

Fig. S5. Relative mass contributions measured with a Q-ACSM (NR-PM_1) and an aethalometer (EBC) in the Swiss Magadino plain. Left: summer 2014 (June, July & August), right: winter 2013 / 2014 (December, January & February).

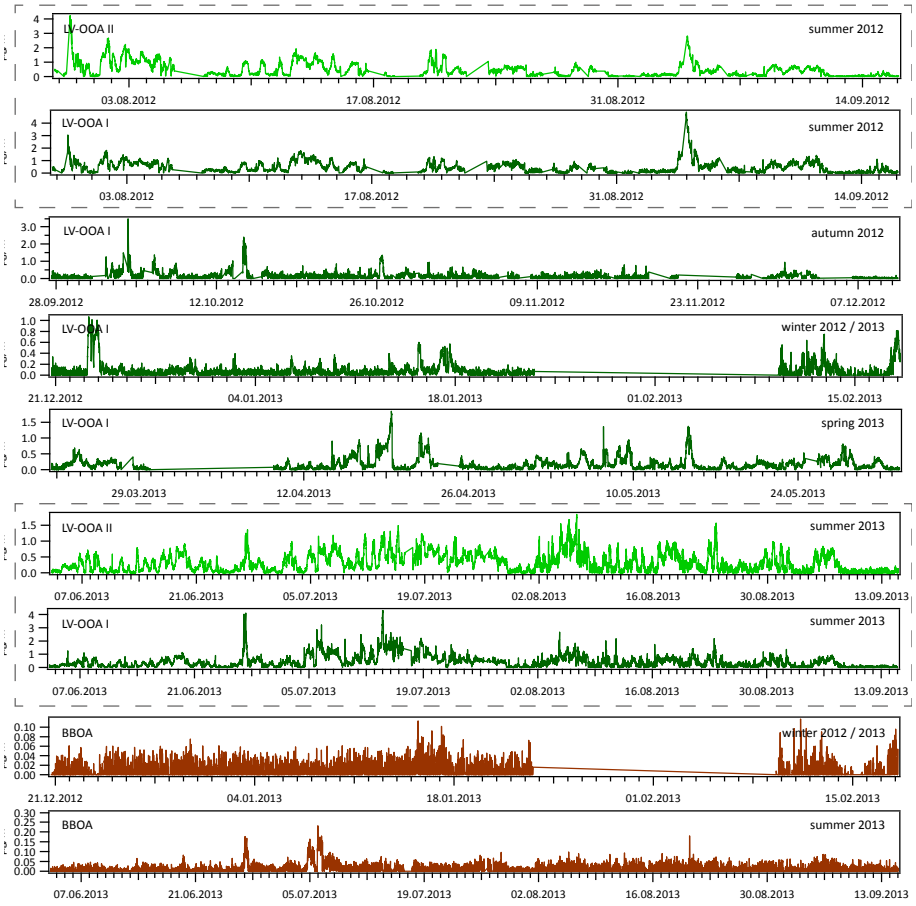

Fig. S6. Time series of ME-2 factors OOA I (dark green), OOA II (light green) and BBOA (brown) for all seasons investigated. BBOA was only identified in winter 2012/2013 and summer 2013.

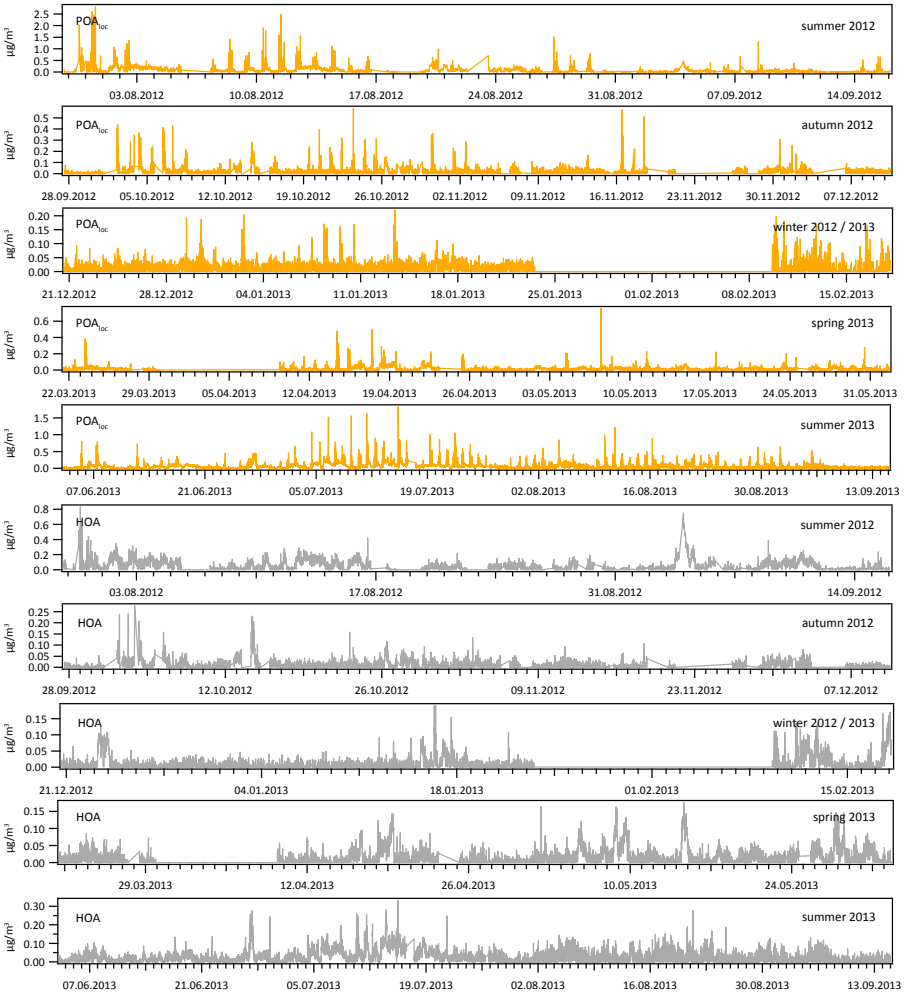

Fig. S7. Time series of ME-2 factors POA_{loc} (orange) and HOA (grey) for all seasons investigated.

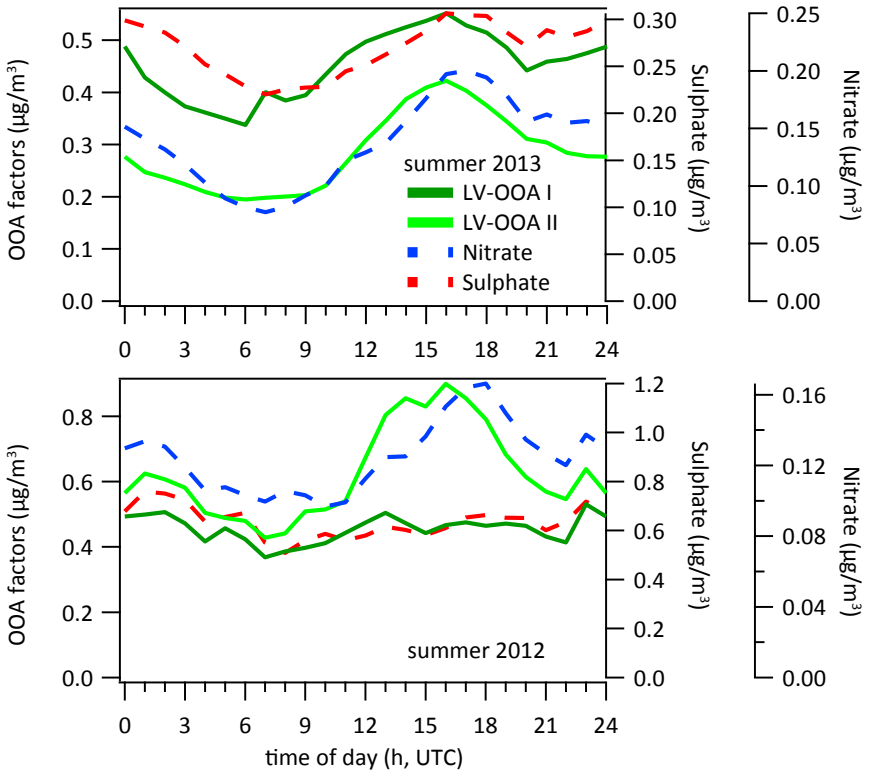

Fig. S8. Diurnal trends of OOA I (dark green), OOA II (light green), SO_4 (red) and NO_3 for summer 2013 (top panel) and summer 2012 (bottom panel).

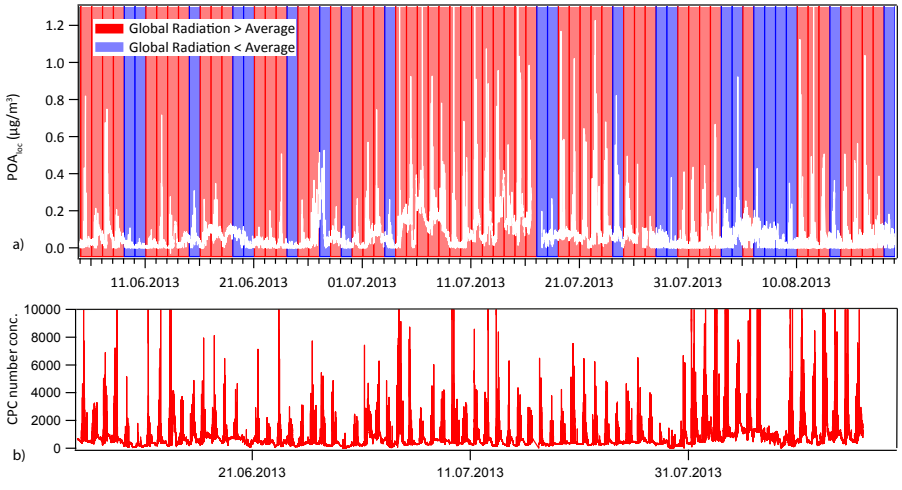

Fig. S9. (a) POA_{loc} (white trace) in summer 2013 with background shaded by average global radiation. Blue (red) means global radiation was below (above) average during that day. (b) CPC number concentrations for the same period.

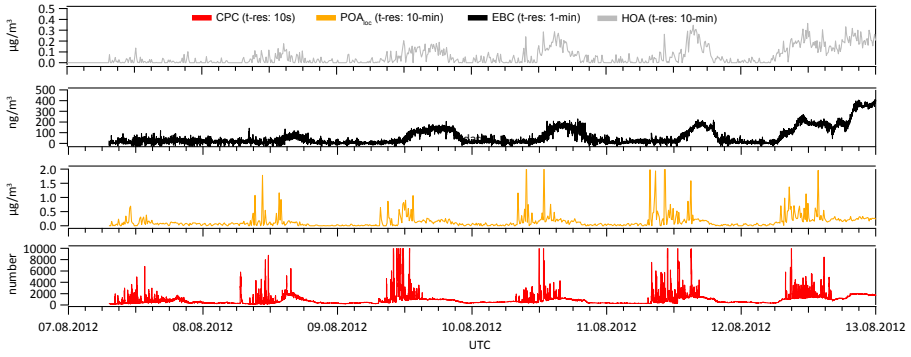

Fig. S10. One-week time series of HOA (grey, time resolution: 10-min), EBC (black, time resolution: 1-min), $\mathrm{POA_{loc}}$ (orange, time resolution: 10-min) and CPC number concentration (red, time resolution: 10-s) in August 2012.

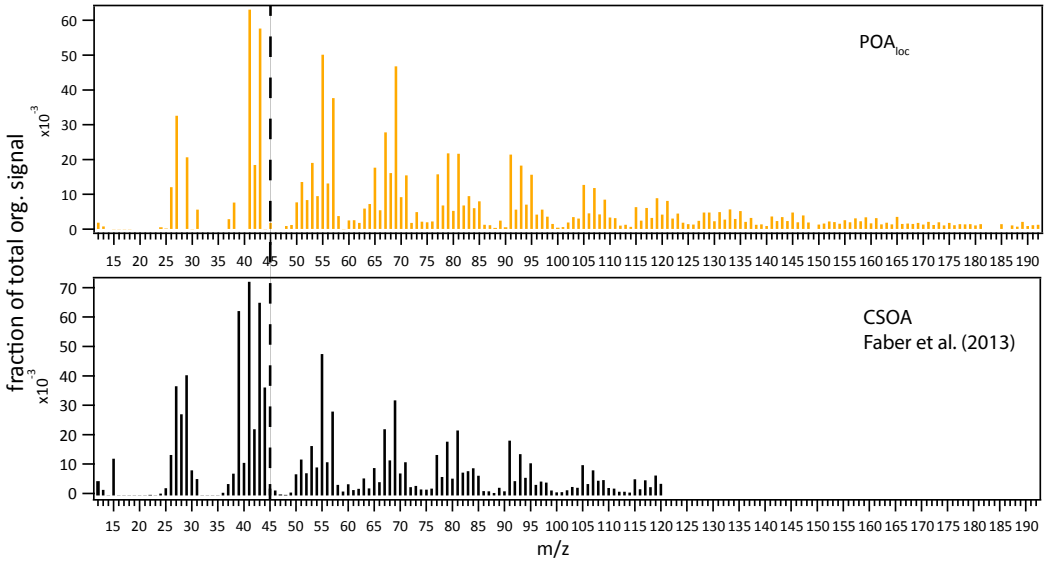

Fig. S11. Top: Mass spectral profile of $\mathrm{POA_{loc}}$, extracted by unconstrained PMF from only short-term peak data. Bottom: Mass spectral profile of cigarette smoke measured with an HR-ToF-AMS under laboratory conditions (adapted and recalculated to UMR from Faber et al., 2013). The CSOA is only shown up to m/z 120. Correlations given in the text are calculated for $m/z > 44$ (dashed line).

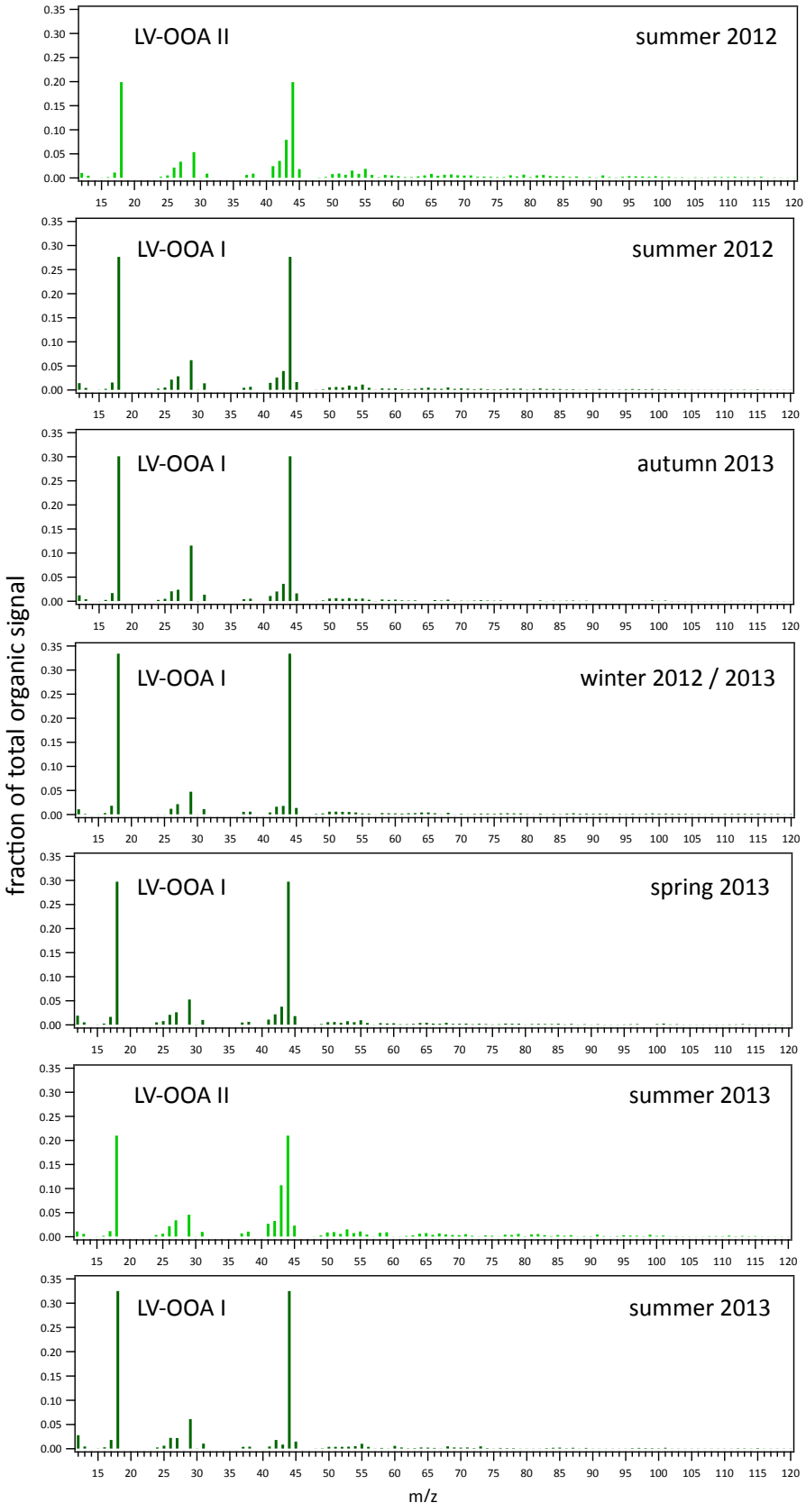

Fig. S12. Mass spectral profile of OOAs for all seasons extracted by ME-2. In both summers OOAs could be split into OOA I (dark green) and OOA II (light green).

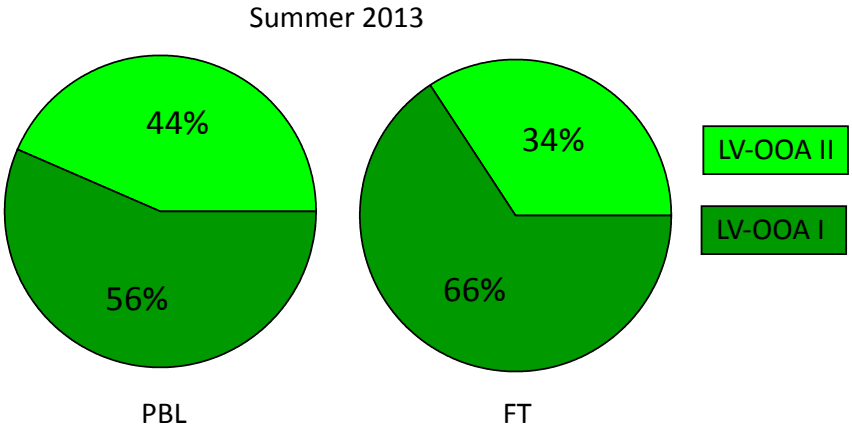

Fig. S13. Relative contributions of LV-OOA I (dark green) and LV-OOA II (light green) in summer 2013 in the FT and with PBL injection.

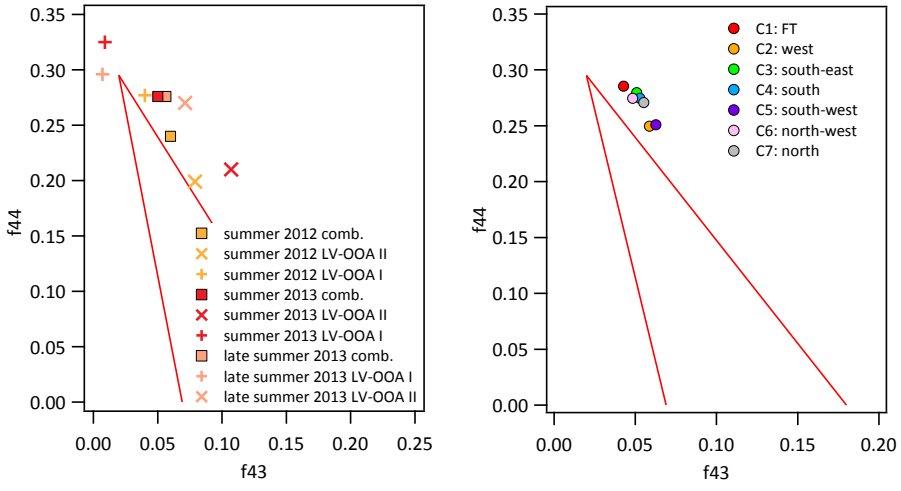

Fig. S14. Triangle plots. Left: Similar to Fig. 9d including data points from a separate ME-2 analysis of only the late summer 2013 overlapping with the summer 2012 period. Right: Triangle plot separated by air mass origin after the subtraction of all POA sources identified in the ME-2 source apportionment. The clusters are the same as in Fig. 5.

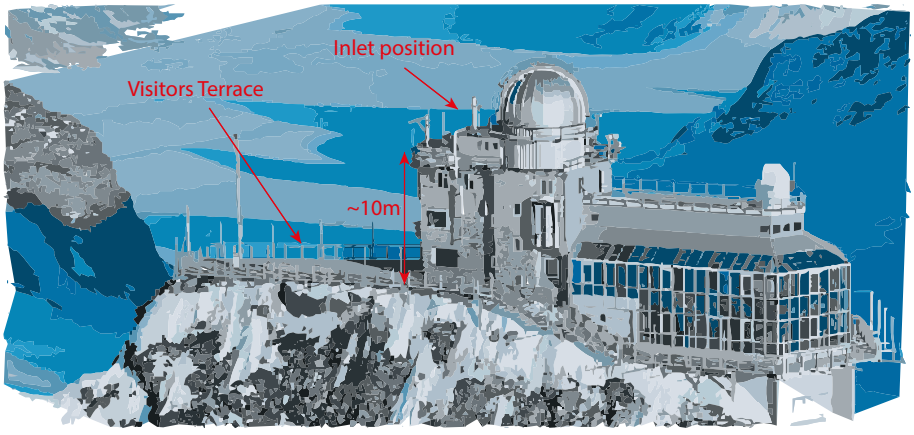

Fig. S15. Sketch of the Sphinx research station at the JFJ showing inlet location and visitors terrace (original image: courtesy of jungfraubahn.ch).

References

Faber, P., Drewnick, F., Veres, P. R., Williams, J., and Borrmann, S.: Anthropogenic sources of aerosol particles in a football stadium: Real-time characterization of emissions from cigarette smoking, cooking, hand flares, and color smoke bombs by high-resolution aerosol mass spectrometry, Atmos. Environ., 77, 1043 – 1051, 2013.